Modelling the interaction of aeolian and fluvial processes with a combined cellular model of sand dunes and river systems

Baoli, Liu[1], Tom, J, Coulthard [2, *]

(1) College of the Environment and Ecology, Xiamen University, Xiamen, China

(2) School of Environmental Sciences, University of Hull, Cottingham Road, Hull, HU6 7RX, UK

* Corresponding Author

Abstract

Aeolian and fluvial processes are important agents for shaping the surface of the Earth, but are largely studied in isolation despite there being many locations where both processes are acting together and influencing each other. Using field data to investigate fluvial-aeolian interactions is, however, hampered by our short length of record and low temporal resolution of observations. Here we use numerical modelling to investigate, for the first time, the interplay between aeolian (sand dunes) and fluvial (river channel) processes. This modelling is carried out by combining two existing cellular models of aeolian and fluvial processes that requires considerable consideration of the different process representation and time stepping used. The result is a fully coupled (in time and space) sand dune – river model. Over a thousand-year simulation the model shows how the migration of sand dunes is readily blocked by rivers, yet aeolian processes can push the channel downwind. Over time cyclic channel avulsions develop indicating that aeolian action on fluvial systems may play an important part in governing avulsion frequency, and thus alluvial architecture.

1. Introduction

1.1 Background and rationale

Fluvial and aeolian processes are important for shaping the surface of the Earth and creating a diverse range of landscapes. Traditionally, field and modelling studies have presented research on *only* fluvial *or* aeolian processes, yet there are many areas where both processes interact with each other in contemporary (e.g. Bourke et al., 2009; Li et al., 1999; Smith and Smith, 1984; Tastet and Pontee, 1998) and paleo settings (Langford and Chan, 1989; Mazzullo and Ehrlich, 1983; Song et al., 2006; Veiga et al., 2002). Only a few researchers have examined fluvial and aeolian interactions, but their studies show a range of interesting interplays and feedbacks between the processes. For example, rivers can act as barriers to sand dunes – stopping their progression - as shown by the Colorado River acting to block the transport of sand from the Mojave Desert (Muhs et al., 2003; Sweet et al., 1988). Conversely, sand dunes can deflect and confine rivers, and in turn define their

position and shape (Langford and Chan, 1989; Loope et al., 1995; Maroulis et al., 2007). River systems can also change pattern and behaviour when they are influenced by aeolian processes by changing from single channel to braided (Smith and Smith, 1984). Sand dunes can also act as a supplier of sediment to rivers – and rivers can in turn lead to the development of dunes where sand is deposited by fluvial action (Langford and Chan, 1989; Maroulis et al., 2007). For example in Sinai in Israel, Roskin et al., (2011) found the sand supply came from the Late Pleistocene exposure of the Nile Delta sands. Contemporary examples of dunes and river systems interacting are shown in the oblique and satellite views of three Chinese systems in Figure 1.

Recently, Liu and Coulthard (2015) compiled a global inventory of 230 sites where there was evidence of both fluvial and aeolian processes operating using satellite imagery, indicating that in arid and semi-arid environments across the Earth such interactions are widespread. However, their research was limited by their use of imagery that only represent single, static moments in time, whereas both sand dunes and rivers are highly dynamic systems. Liu and Coulthard's (2015) research leaves a set of unanswered questions concerning the *dynamic* interaction of aeolian dunes and rivers. How do sand dunes alter rivers over time? How do rivers in turn alter sand dunes? How can each disrupt or interact with the other? How do sand dunes cross over a river system? Are there distinctive landforms or patterns left by these interactions – and how well does the static interpretation reflect the dynamic?

Such questions can only be partly answered by using field data as the rates of change (i.e. dune movement) in aeolian and fluvial systems are often too slow to generate a meaningful record within our limited range of observations. In addition, the periodic nature of observation (e.g. remotely sensed imagery) will likely miss events that are important in the system evolution, such as changes associated with floods or storms. An alternative approach would be to use numerical modelling to allow us to simulate the dynamic interactions between dune and river processes and examine *how* landforms evolve and what can control them.

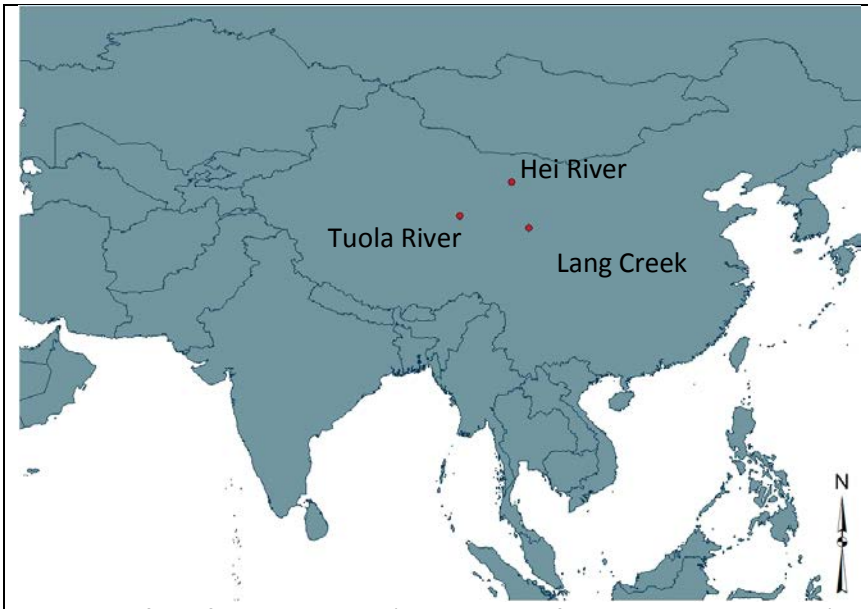

Location of the field examples. (Photo credit for all images: Baoli Liu)

Legend: ● location photo was taken from – shaded triangle indicates the image field of view.

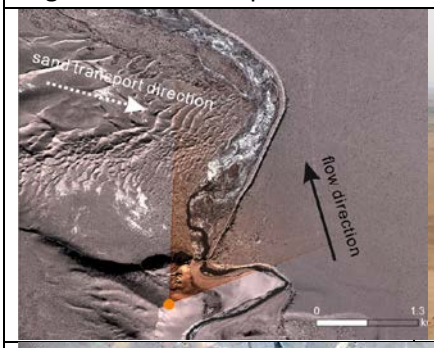

Hei River:

Dune movement appears restricted by the channel, and dunes on the edge of channel are eroded and modified by the water.

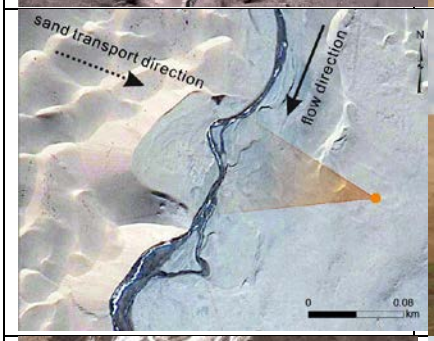

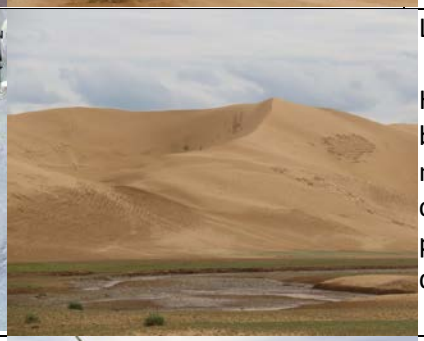

Lang Creek:

Here, dunes are located on both sides of the channel but much larger dunes stop at the channel, indicating that fluvial process are preventing the dunes passage.

Tuola River:

An example of a barchan dune that has crossed over the channel

Figure 1. Aerial and oblique images of river and sand dune interactions from China. Here, these examples from the field are used to illustrate that the morphologies generated in the combined model of sand dunes and river systems are similar to those found in nature.

61

62 **1.2 Numerical modelling of sand dunes**

63 There is a long history of numerical modelling for aeolian dunes (Bishop et al., 2002; Howard et al.,
64 1978; Hugenholtz et al., 2012; Kroy et al., 2002; Livingstone et al., 2007; Nishimori et al., 1998;
65 Ouichi and Nishimori, 1995; Parteli and Herrmann, 2003; Wippermann and Gross, 1986). Notable
66 approaches include the use of simple cellular automata type models by Werner (1995), Nishimori et
67 al., (1998) and Ouichi and Nishimori (1995) that have been used to show the development and
68 dynamics of sand dunes. These cellular models assumed that a dune field can be represented by
69 moving 'slabs' of sand in a down wind direction over a mesh of square grid cells. These slabs can pile
70 up and lead to a 'shadow zone' in the downwind direction where slabs cannot be moved.
71 Additionally, when the slabs pile up to a height leading to slopes that exceed a threshold angle they
72 can landslide down. When iterated the slab piling leads to accumulation on the upwind side and
73 landslides on the downwind, enabling dunes to form and migrate downwind (Werner, 1995). By
74 varying the sediment supply and wind direction slab models can be made to replicate the
75 development of barchan, transverse ridge, linear and star dunes (Barchyn and Hugenholtz, 2012;
76 Bishop et al., 2002; Werner, 1995). Werner and Nishimori's work has since been extensively built
77 upon and used by a number of researchers (e.g. Baas and Nield, 2007; Bishop et al., 2002; Eastwood
78 et al., 2011; Momiji and Warren, 2000; Narteau et al., 2009; Pelletier, 2009; Zhang et al., 2012).

79 More complex methods for simulating sand dune development have been developed (e.g. Parteli et
80 al., 2014; Zhang et al., 2012) but the attraction of the simple cellular models described above is that
81 their parsimony and numerical efficiency allows their application to larger spatial areas and over
82 longer time scales. Such model parsimony can make integration with other, e.g. fluvial models much
83 more straightforward.

84 **1.3 Numerical modelling of river systems**

85 In the past decades, a wide range of numerical models have been developed to simulate the
86 morphological development of river systems over a range of temporal and spatial scales, from
87 decades to millennia, from reach scale to catchment scale. These models often focus on different
88 aspects of fluvial systems, e.g. channel network models, models of river meandering and river
89 braiding, alluvial stratigraphy models, and landscape evolution models (LEMs) (Coulthard, 2001;
90 Coulthard and Van De Wiel, 2012; Tucker and Hancock, 2010). The computational simulations of the
91 landscape evolution have been especially helped by adoption of cellular approaches (Coulthard et
92 al., 2007; Murray and Paola, 1997, 1994; Nicholas, 2005; Willgoose, 2005) where the landscape and
93 landforms are represented by a grid of cells and their evolution simulated by the routing of water

and sediment over this gridded landscape. Other examples of such cellular or 'reduced complexity' models (Larsen et al., 2014) include the braided river model of Murray and Paola (1994; 1997) the river models of Thomas and Nicholas, (2002) , Castelltort and Van Den Driessche (2003) and the CAESAR-Lisflood model (Coulthard et al., 2013). A notable feature of these cellular models is their use of simplifications of largely empirical relationships to calculate water and sediment fluxes. Whilst this simplification may not have the stronger physical basis of Navier-Stokes approaches their parsimony makes their operation far more computationally straightforward. In turn this makes cellular models considerably faster enabling them to simulate larger areas, at more detailed spatial resolutions and for longer time scales. Like the dune models described above, their strength lies not in their predictive capability, but their ability to simulate the dynamics and behaviour of the system.

1.4 Summary

The above summarise only a small part of the considerable body of research concerning the numerical modelling of river systems and for sand dunes. However, considering this and the wider literature there are to date no studies that have attempted to fully combine numerical models of sand dunes and river systems. In this paper, we describe how two contemporary cellular aeolian and fluvial models were fully coupled including the reconciliation of different process rates, scales and representations in the two codes. Finally, we present several examples that illustrate the combined models versatility and its use in investigated Aeolian/Fluvial systems.

2. Model descriptions

2.1 CAESAR-Lisflood

CAESAR-Lisflood (Coulthard et al., 2013) is a landscape evolution model with an integrated hydrological and hydraulic model that operates on a sub-event time scale, featuring multiple grainsize erosion and deposition as well as including slope processes (soil creep and landslides). CAESAR-Lisflood was originally developed to examine the relative importance of climate and land-cover change on catchment morphology and sediment discharge. It has been applied to a wide range of river catchments and reaches with the outputs successfully compared to independent field data (e.g. Coulthard and Macklin, 2003, 2001; Coulthard et al., 2012; Hancock et al., 2010; Welsh et al., 2009).

CAESAR-Lisflood simulates landscape development by routing water over a grid of regular-sized cells and changing elevations to simulate erosion and deposition from fluvial and slope processes. CAESAR-Lisflood needs several parameters or initial conditions including surface elevation, grain

sizes and rainfall (catchment mode) or a flow input (reach mode). In principle, its operation is simple, where modelled flow drives fluvial and hillslope processes that determine the erosion and deposition for the modelled time step. These processes change the topography, which then becomes the starting point for the following time step. There are four main components in CAESAR-Lisflood, a hydrological model (not described here), a surface flow model, fluvial erosion and deposition and slope processes.

2.1.1 CAESAR-Lisflood flow model

In this application, the hydrological model is not utilised as surface water is added directly at one side of the modelled domain. Where added, this surface water is routed using the Lisflood-FP flow model (Bates et al., 2010) to the four cells in the x and y directions according to equation 1

$$q_{t+\Delta t} = \frac{q_t - g h_{flow} \Delta t \frac{\partial (h_t + z)}{\partial x}}{\left(1 + g h_{flow} \Delta t n^2 q_t / {h_{flow}}^{10/3}\right)} \qquad (1)$$

Here, Δt = length of time step (s); t and $t + \Delta t$ are the present time step and the next time step; q = flow per unit width (m^2/s); g = gravitational acceleration ($m\ s^{-1}$); h = flow depth (m); z = bed elevation (m); and x = grid cell size (m); $\frac{\partial (h_t + z)}{\partial x}$ = water surface slope and h_{flow} is the difference in elevation between the maximum water surface elevation and maximum bed elevation of the two cells where water is being routed between.

To maintain numerical stability (due to instability from water being moved too fast between cells) the model time step at $t + \Delta t$ is calculated by Equation 2, where α is the Courant number typically defined between 0.3 and 0.7 (Bates et al., 2010; Coulthard et al., 2013).

$$\Delta t_{\max} = \alpha \frac{\Delta x}{\sqrt{g h_t}} \qquad (2)$$

When flow rates between cells have been calculated using Equations 1 and 2 water depths for all cells are updated simultaneously and the model then calculates fluvial erosion and deposition.

2.1.2 Fluvial erosion and deposition in CAESAR-Lisflood

CAESAR-Lisflood models fluvial erosion, transport and deposition of multi grainsized sediment by using up to nine grain size fractions that are integrated within a 3D active layer system that contains one surface active layer and multiple buried layers (Coulthard et al., 2013; Coulthard and Van De Wiel, 2007; Hancock et al., 2010; Van De Wiel et al., 2007). These active layers contain quantities of sediment for each of the nine size fractions and sediment is passed between the layers during

erosion and deposition allowing the development of features such as an armoured channel bed and a stratigraphy (Coulthard and Van De Wiel, 2007; Van De Wiel et al., 2007).

The thickness of the buried layers is fixed by the parameter L_h. The thickness of the surface active layer can vary between 25% and 150% of L_h and acts as a buffer between erosion and deposition on the channel bed and the strata layers below. If the thickness of the active falls below 0.25 L_h (for example during erosion) then the upper strata layer is incorporated into the active layer. Alternatively, if (for example during deposition) the active layer exceeds 1.5 L_h, the active layer is split so the layer below receives 1 L_h (Van De Wiel et al., 2007).

The amount of sediment eroded by fluvial action can be calculated using two different methods, based on either the Einstein (1950) or the (Wilcock and Crowe, 2003) transport equations (Coulthard et al., 2013). For the Einstein (1950) method, calculation of sediment transport for each size fraction i requires the calculation of the balance between the forces moving and restraining a particle (Equation 3)

$$\psi = \frac{(\rho_s - \rho)D_i}{\rho dS} \quad (3)$$

Where the term ρdS is replaced by τ/g. A dimensionless bedload transport rate ϕ is then estimated from ψ using the relationship (Equation 4) described by Einstein (1950).

$$\phi = 40(1/\psi)^3 \quad (4)$$

The value of ϕ is then used in Equation 5 to estimate q_i, the rate of sediment transport (m^3s^{-1}):

$$\phi = q_i \sqrt{\frac{\rho}{(\rho_s - \rho) g {D_i}^3}} \quad (5)$$

For the Wilcock and Crowe (2003) method, sediment transport rates (q_i) for each sediment fraction (i) are determined by Equation 6.

$$q_i = \frac{F_i U_*^3 W_i^*}{((\rho_s - \rho) - 1)g} \quad (6)$$

Here F_i is the fractional volume of the i-th sediment in the active layer, U_* is the shear velocity ($U_* = [\tau/\rho]^{0.5}$) and W_i^* is a function that relates the fractional transport rate to the total transport rate (Van De Wiel et al., 2007). In order to calculate W_i^*, it is first necessary to calculate τ_{rm}, a critical shear stress for the mean size of the bed sediment. τ_{rm} is determined by a function that the relates Shield's parameter for the mean bed material size (τ_{rm}^*) to the percent of sand on the bed surface (F_s) as per Equation 7.

$$\tau_{\mathrm{rm}}^* = 0.021 + 0.015 \exp[-20F_s] \quad (7)$$

The dimensionless value τ^*_{rm} can then be converted to shear stress (Nm^{-2}): $\tau_{\mathrm{rm}} = \tau^*_{\mathrm{rm}} \rho g D_{s50}$ and in Equation 8 rearranged to calculate τ_{ri}, the reference or critical shear stress for the i-th size fraction:

$$\frac{\tau_{\mathrm{ri}}}{\tau_{\mathrm{rm}}} = \left(\frac{D_i}{D_{s50}}\right)^b \quad (8)$$

Where b is an exponent determined in Equation 9.

$$b = \frac{0.67}{1+\exp\left(1.5-\frac{D_i}{D_{sm}}\right)} \quad (9)$$

W_i^* is then be calculated as in Equation 10,

$$W_i^* = \begin{cases} 0.002\phi^{0.75} & \text{for } \phi < 1.35 \\ 14\left(1-\frac{0.894}{\phi^{0.5}}\right)^{4.5} & \text{for } \phi \geq 1.35 \end{cases} \quad (10)$$

Here $\phi = \tau/\tau_{\mathrm{ri}}$. W_i^* is then substituted into the main equation to obtain sediment transport rate q_i (m^{3}s^{-1}).

The calculation of shear stress (τ) that drives both the Einstein (1950) and Wilcock and Crowe (2003) formulations within CAESAR-Lisflood is determined from square of the resultant flow velocity v^2 (Equation 11) the drag coefficient Ci and a constant (1000).

$$\tau = 1000\, Ci\, v^2 \quad (11)$$

The amount of sediment transported is multiplied by the time step ($\mathrm{d}t$). However, as CAESAR-Lisflood has a variable time-step, $\mathrm{d}t$ is controlled by a variable that specifies the maximum change in elevation that is allowed during an iteration, ΔZ_{max}. This parameter is used to calculate the time step in Equation 12, where q_{max} is the maximum transport rate calculated for a given iteration, and Dx is grid cell size.

$$\mathrm{d}t = \frac{\Delta Z_{\mathrm{max}} Dx^2}{q_{\mathrm{max}}} \quad (12)$$

Equation 12 ensures that the time step reduces to short periods (e.g. less than a second) during periods of intense geomorphic activity, but extends to an hour during periods of stability (Van De Wiel et al., 2007).

2.1.3 Lateral erosion

Lateral erosion (for example, bank erosion leading to channel migration) is represented in CAESAR-Lisflood (after Coulthard and Van De Wiel, 2006) using a lateral erosion algorithm driven by the local radius of curvature (R_{ca}) calculated on a cell-by-cell basis (Coulthard and Van De Wiel, 2006).

Equation 13 then determines lateral erosion (ζ) based on R_{ca}, Λ (lateral erosion rate – user defined parameter), τ (shear stress of the cell adjacent to the bank) and T (time).

$$\zeta = \frac{1}{R_{\mathrm{ca}}} \Lambda \tau T \qquad (13)$$

Material eroded from a bank cell is then deposited in the cell next to the bank and then redistributed via regular fluvial erosion and deposition. To simulate the lateral movement of sediment across channels (for example, to simulate deposition along the inside bank of the meander bend) sediment is also moved using a cross-stream gradient calculated by interpolating values of R_{ca} across the channel (Van De Wiel et al., 2007). As this algorithm assigns negative R_{ca} values to cells on the inside bank and positive R_{ca} values to cells on the outside bank, a cross-stream gradient can be determined by interpolating the R_{ca} values across the channel (Van De Wiel et al., 2007). A lateral sediment flux Ψ_n can then be calculated from this cross-stream gradient (Equation 14).

$$\Psi_n = a\left(R_{ca,n} - R_{ca,n-1}\right)h_n \qquad (14)$$

Here, *n* and $n-1$ are the donor cell and the receiving cell, *a* is a coefficient and *h* is the flow depth (Van De Wiel et al., 2007). To maintain the downstream migration of meanders and lateral erosion, CAESAR-Lisflood shifts the previously calculated cross-channel gradient downstream by several cells denoted by the user.

2.1.4 In-channel lateral erosion

Distinct from the lateral erosion method described above, the in-channel lateral erosion rate acts to control channel geometry by adding to a cell that has experienced erosion material from adjacent in-channel cells. This in channel erosion effectively diffuses channel bed erosion and is designed to prevent positive feedbacks leading to deep single thread channels. The volume of material moved from the donor cell is dependent on the in channel lateral erosion rate and the slope between cells (Equation 15).

$$\Delta Z_{n-1} = \frac{E_{n-1}\,\lambda(Z_n - Z_{n-1})}{Dx} \qquad (15)$$

Here *n* and $n-1$ denote the donor and the receiving cells, Z is cell elevation, δZ is the change in cell elevation, E is the volume of material eroded, λ is in-channel lateral erosion rate and Dx is grid cell size.

2.1.5 Slope processes

Mass movement or landslides within CAESAR-Lisflood are simulated as an instantaneous removal process where once the slope between two adjacent cells exceeds a defined threshold material is moved from the uphill cell to adjacent downhill (Coulthard et al., 2002).

Soil creep (m) is also modelled with a diffusion-like processes whereby sediment flux is linearly proportional to surface slope (Carson and Kirkby, 1972) as in Equation 16, where C_{rate} is the user-specified rate of soil creep (m yr^{-1}) and T = time (years).

$$Creep = \frac{SC_{\mathrm{rate}}T}{Dx} \qquad (16)$$

The inclusion of both mass movement processes within CAESAR-Lisflood allows material from hill slopes to be fed directly into the fluvial system from both smaller scale processes, such as bank collapses, and larger scale processes including landslides (Hancock et al., 2011).

2.2 DECAL model overview

The aeolian model used is based on Werner's (1995) non-dimensional 'slab' dune model (DECAL) as implemented by Baas (2002) and Nield and Baas (2008).A brief description of the dune models operation is provided below and in Figure 2.

Aeolian sand is moved in slabs of a fixed depth (h) and moved in one direction (assumed to be down wind) by a set of simple rules. Firstly, a grid cell is randomly selected from the modelled domain and if there is a slab in that cell that can be entrained (i.e. does not lie within a shadow zone – or under the influence of an upwind feature: Figure 2) then the slab is moved downwind a constant transport length l (measured in grid cells and here set to 1). At the new downwind location, the slab is either deposited or moved another distance downwind per the deposition probability (P_d). This process is repeated until the slab is deposited. Additionally, a slab must be deposited if it falls into a shadow zone on the leeward side of a dune during the above sequence ($P_d = 1$). The selection of random cells continues until the total number of cells selected equals the size of the modelled domain, thus allowing most cells to be accounted for. Throughout this process an angle of repose (default 30°) is enforced so any over steepening of dune faces leads to an avalanche until the face is below the threshold (using the landslide function of CAESAR-Lisflood). This combination of movement enables sand to pile up creating a shadow zone that then limits transport and erosion in the downwind 'shadow' area, which further allows sand to pile up into a dune shape. The dune then continues to migrate downwind due to the avalanching of sand down its leeward face.

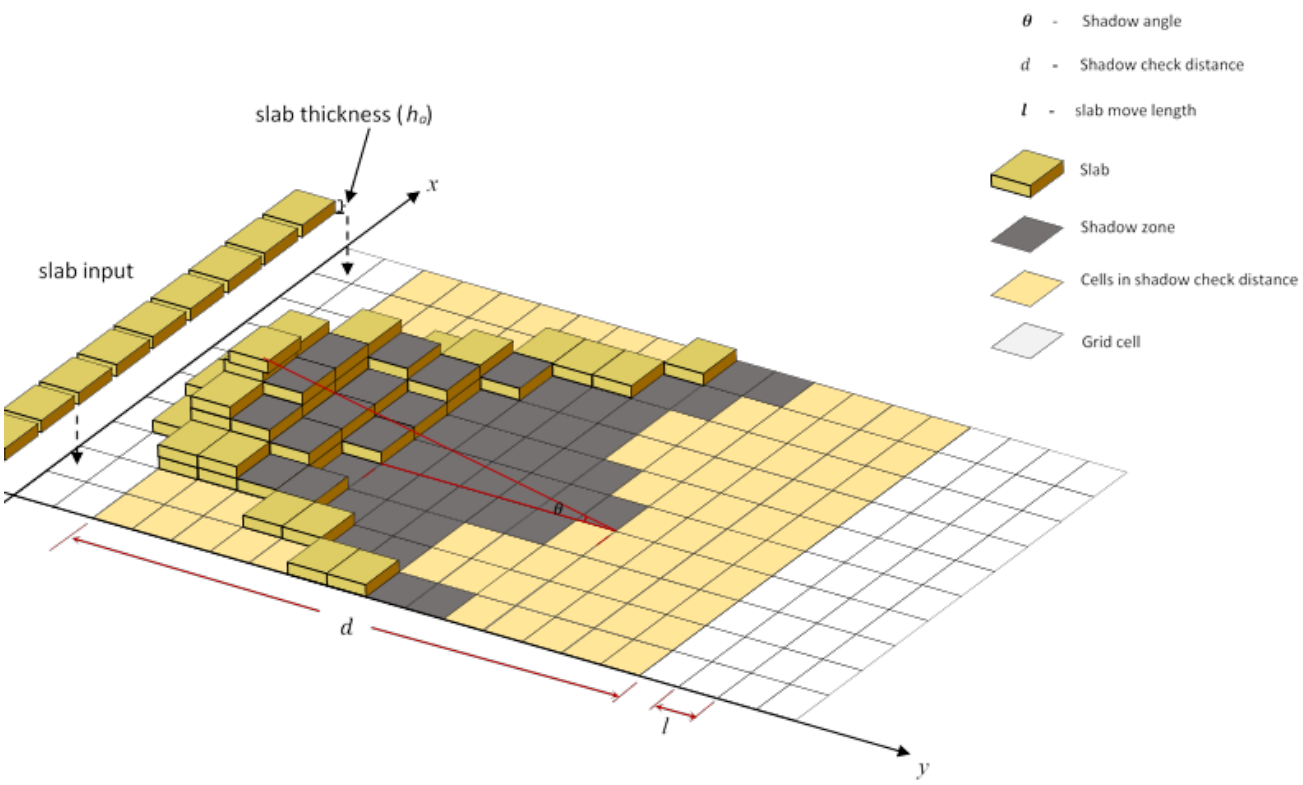

Figure 2. Schematic of the DECAL model operation and parameters.

2.4 Linking CAESAR-Lisflood and DECAL

Merging the DECAL dune model with CAESAR-Lisflood required a series of important modifications but did not change the model equations and procedures outlined above. Rather than write a new bespoke code the equations from the DECAL model were embedded within the CAESAR-Lisflood code that is written in C#.

Both models operate over a regular square grid mesh and share the same DEM of elevations so changes in elevation caused by either DECAL or CAESAR-Lisflood can easily be fed into the other model. For example, sand moved by aeolian processes may cause the river to change course (as the grid cell is higher) or add sediment to the river (if the fluvial model erodes that cell). Similarly, material deposited by the river may be moved as aeolian sediment. As CAESAR-Lisflood contains multiple grainsizes, aeolian sediment moved by DECAL corresponds to the finest grainsize fraction in CAESAR-Lisflood and all the other grainsizes are saved for fluvial erosion and deposition.

For integrating the models, two additional simple rules are applied to the DECAL model whereby slabs of sand cannot be moved if they are under water – and if slabs being transported by DECAL

encounter water they are instantly deposited. These rules prevent sediment being entrained by DECAL when cells are wet and stops sand traversing or being blow across streams. In the field there will be examples where sand is carried over bodies of water, however we argue that the model rules are largely correct where the bulk of aeolian transport is by saltation and grid cells sizes are comparatively large (e.g. > 10m).

There are two important issues that needed overcoming in the model integration related to different model time steps and the depth of slabs used by DECAL. Because the aeolian sand is moved in slabs there is a significant difference between the time steps required for aeolian and fluvial models to move appropriate amounts of sediment and therefore the dune model has a longer time step. For example, each iteration of the sand dune model may represent 10 days of aeolian transport whereas each iteration of the fluvial model may only be a few seconds. In CAESAR-Lisflood, the shorter time step of the fluvial model is required to maintain numerical stability (see Equation 12 above). To overcome this difference in time steps, the fluvial components are run repeatedly until, for example, 10 days of simulated time has elapsed then the dune model operates – then fluvial components for another 10 days and the process repeats. Effectively, the two models operate at two different speeds with the dune model called every 10 days whilst the fluvial model operates continuously. The 10 day repeat is just for the example described above and can readily be changed.

A key feature of DECAL is that the movement of sand as *slabs* of sediment (e.g. slabs of sand 0.5m thick in this study) vital for the formation of sand dunes within the model. For example, if one or more slabs are deposited on top of each other this creates a shadow areas that in turn leads to a reduction in aeolian transport downwind and thus the starting point for a modelled dune. However, if the slabs are too small, then the shadow areas are negligible and no dunes will form – in effect sand will move as a sheet. The dune model is therefore dependent upon the thickness of the slabs to create shadow areas. However, in our example, relative to the fluvial components, substantial volumes of sand are moved for every iteration of DECAL (i.e. on 10m grid cells, a single slab is 10m x 10m x 0.5m).

Unfortunately, both of these issues lead to a further problem as the comparatively thick slabs of aeolian transported sand can effectively be dumped ‘instantaneously’ into the channel leading to channels to becoming suddenly blocked or dammed. To overcome this, the sand movement from DECAL in slabs (e.g. 0.5m depth) is calculated every 10 days (for example) but the changes in elevation from this are applied gradually at every hour of simulated time over the following 10 days of model operation (0.5m / 240). The net result is a fully coupled integration of the two models – with the fluvial model able to interact and feed back to the aeolian model and vice versa.

3 Simulation configuration

The results described in this paper are from a single 1000 year-long simulation selected to provide examples of the dynamic morphological interactions that the combined models can generate of fluvial and aeolian processes. Continuous and non variable aeolian transport rates and water discharges were used which we recognise are un-realistic, but provide a parsimonious model configuration within which to evaluate how the models interact. The model version used was CAESAR-Lisflood 1.9b (Coulthard, 2017). Parameters used to drive the flow model are detailed in Table 1 and for the aeolian model in Table 2, equating to a rate of 102 $m^3m^{-1}yr^{-1}$.

Table 1 Fluvial model parameters

Flow model parameter	**Value**
Erosion law	Wilcock and Crowe (2003)
Max erode limit	0.005
Active layer thickness (*m*)	0.05
Lateral erosion rate	0.000002
Water depth threshold above which erosion will happen (*m*)	0.01
Evaporation rate (*m/day*)	0.0005
Courant number	0.5
Hflow threshold	0.001
Mannings number	0.04
Discharge (m^3s^{-1})	5

Table 2 Aeolian model parameters

Parameter	**Units**	**Value**
h_a	*metre*	0.3
h_s	*metre*	0.5
θ	*degree*	10
d	cell	60
P_d	%	65
t	*minute*	14400

Sand flux rate	$m^3m^{-1}yr^{-1}$	102

331

332 The simulation was carried out over a model domain of 500 by 200, 10m square grid cells. These
333 were set with a downstream gradient of 0.005 and a lateral gradient of 0.0005 to gently direct water
334 towards the centre line of the modelled area. For model boundary conditions water and sediment
335 was introduced at the upstream (LH) side of the DEM. Sediment inputs were derived by running the
336 model in fluvial only mode for 10 years generating a time series of sediment outputs – that were
337 then used as inputs. If no sediment inputs were used the channel (of clean water) would incise at the
338 upstream end.

339

340

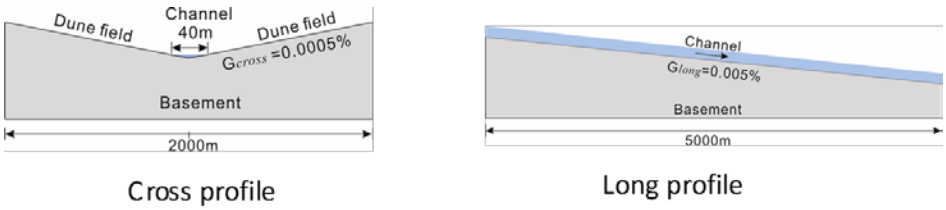

341

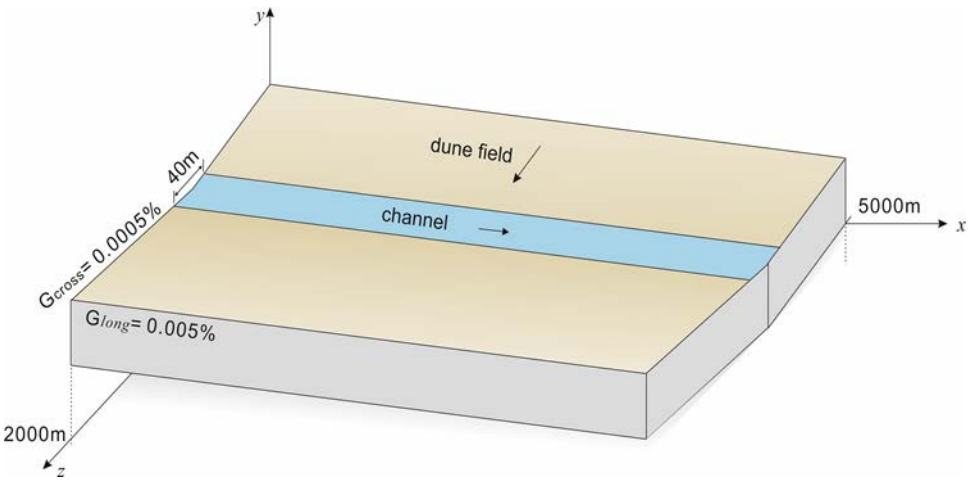

342

343 *Figure 3 Schematic illustration of modelled domain illustrating model slopes, dimensions and*
344 *direction of sand and water inputs.*

345 Previous workers have noted a sensitivity of the DECAL model to input conditions (Baas, 2002;
346 Eastwood et al., 2011; Nield and Baas, 2008) and use a periodic (recirculating) sand boundary
347 (Werner, 1995). As in this experiment fluvial and aeolian sand can mix and therefore be transported
348 over the right or lower edge, we are unable to use a periodic boundary. Consequently, the model
349 was set to have fresh sand entering the model space along the upwind border (top) and exiting at
350 the lower downwind edge of the modelled domain. Aeolian sand leaving the bottom edge of the
351 modelled domain is recorded separately from fluvially moved sand leaving the right hand edge
352 enabling aeolian and fluvial outputs to be separately recorded. Elevations, images, water and
353 sediment discharges can be recorded at user specified intervals.

354 **4. Results**

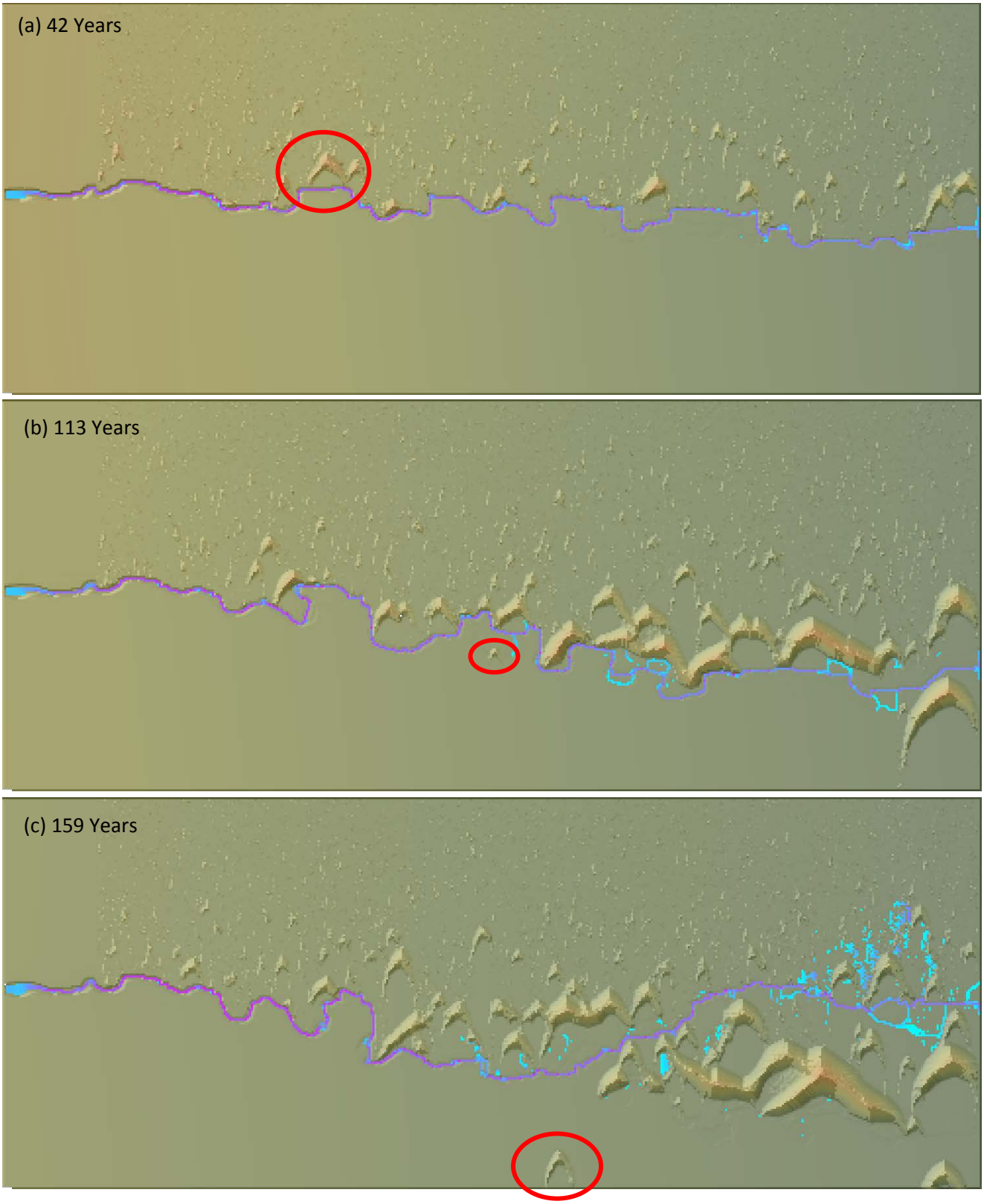

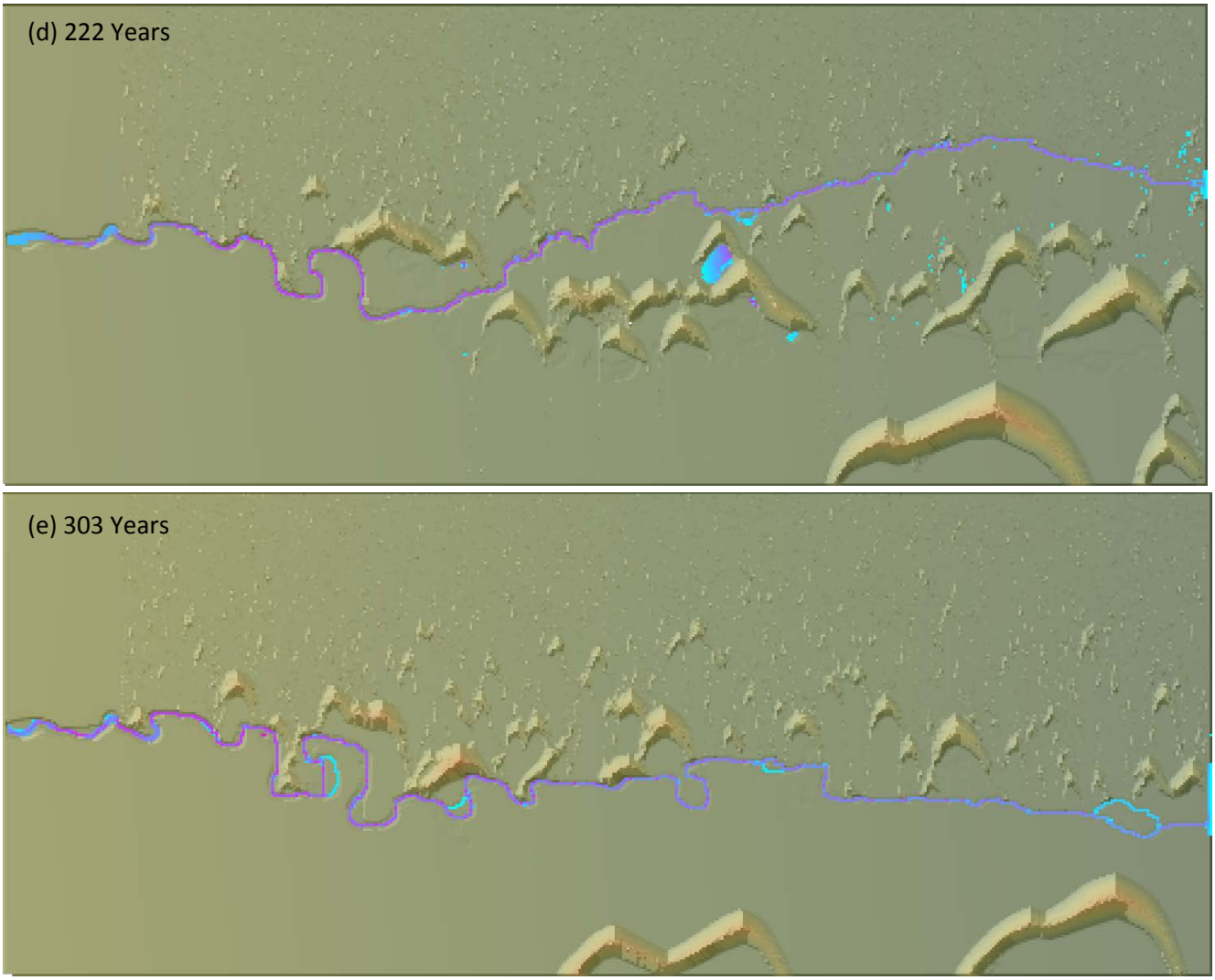

355

356 *Figure 4 images of channel and dunes interacting at 5 time slices during the 1000 year simulation.*
357 *Photographs and satellite images of similar dune/river behaviour in the field are provided in Figure 1.*

358 Figure 4 shows the surface morphology and position of the channel for five time slices of the
359 simulation. In all images, fluvial flow is from left to right and aeolian from top to bottom. In the
360 descriptions, upstream refers to the left of the images, downstream the right, upwind the top and
361 downwind the bottom.

362 At 42 years, Figure 4A shows the channel has formed a gently meandering planform and sand dunes
363 (barchan) have formed upwind of the channel. However, the channel has prevented sand from
364 crossing forming a barrier to dune migration. By 113 years, (Figure 4B) the channel has continued to
365 migrate and develop, but further downstream the cumulative effect of the aeolian transport and
366 dunes colliding with the river has caused the channel to become deflected in a downwind direction.
367 Aeolian transport raises the upwind bank relative to downwind making it easier for the channel to

move downwind. However, the channel is capable of consuming sand dunes as shown by the removal of the barchan dune circled in Figure 4A. However, a very small barchan dune (circled) has managed to cross the river – due to sufficient sand being deposited from the river being re-worked to generate a new dune on the downwind side. Figure 4C (159 years) shows how dunes in the downstream end of the domain have raised elevations enough to cause the lower part of the stream to avulse in an upwind direction where there are smaller, lower, less obstructive dunes – enabling a large group of dunes to cross the stream. In addition, another barchan dune (circled) has crossed via the reworking of fluvial sediment as detailed above. By 222 years (Figure 4D) a second phase in the avulsion is shown where the upstream part of the channel has moved upwind. Both avulsions (Figures 3C and 3D) allow a large area of dunes to effectively cross the river in one group or set. Finally, by 303 years (Figure 4E) the process repeats with the channel aligned approximately centrally and a set of dunes beginning to develop upwind of the channel as per Figure 4A. The interactions and morphologies shown in the above simulations correspond with those observed in the field (Figure 1).

5. Discussion

The simulation results presented clearly show that the combined model can capture the dynamic interactions between fluvial and aeolian generating morphologies and landscapes similar to those observed (e.g. Figure 1). The basic simulations presented here provide us with novel insight into the interactions of the two processes that have important implications for how we interpret and understand landscapes where there are fluvial/aeolian interactions. Two straightforward interactions are responsible for all the landscapes simulated here (1) the ability of the fluvial flow to absorb aeolian fluxes and largely stop the progress of sand dunes and (2) aeolian sand fluxes being capable forcing the channel to migrate and avulse.

Firstly, the ability of small perennial flows to restrict/stop sand dunes was unexpected. Compared to observations (Liu and Coulthard, 2015) our water/fluvial inputs are very low and our sand transport rates very high (100 $m^3m^{-1}yr^{-1}$ compared to 76-99 $m^3m^{-1}yr^{-1}$ observed, Vermeesch and Drake, 2008)). Secondly, despite dunes being restricted/stopped by channels, aeolian transport can push the channel laterally. By raising elevations upwind of the river, the downwind bank is relatively lower and thus easier for the channel to migrate downwind. Over time, the cumulative effect of this process is that as the channel is pushed further laterally from its original path until the gradient becomes sufficiently low that it seeks a steeper path of descent avulsing back towards its original path.

The driving of river avulsion by aeolian processes is a highly significant finding. Avulsions are a fundamental process in the development of alluvial aquifer structures (for both water, gas and oil) and there are few field observations of aeolian forced avulsions (e.g. Hollands et al., 2006; Jones and Blakey, 1997). In our simulations avulsions are widespread and could have very important implications for our interpretations of stratigraphies, especially from the Paleozoic period where there was no vegetation (Davies and Gibling, 2010a, 2010b). Interestingly, these 'nodal avulsions' happen in two stages in our simulations (Figure 4 B and C), have a directional bias linked to the prevailing wind direction and may be cyclical. Furthermore, avulsions enable dunes to migrate across channels en-mass by the channel re-forming upwind of the dunes. Dunes were also able to pass channels by the translocation of sediment where sand from the river deposited overbank (originally sourced via fluvial or aeolian) could lead to the re-formation of dunes down-wind of a river. However, in our examples, translocation led to much smaller dunes crossing a river and therefore channel avulsion appears a far more effective process to allow dunes or a mass of aeolian sediment to pass.

It is Important to remember that these simulations are configured with perennial flows of water and sand and do not consider any impacts that changing frequency and magnitude of sediment fluxes might cause. Furthermore, the directions of flow (aeolian and fluvial) are fixed. In these experiments sand transport rates are very high – but they are continuous, whereas in reality similar annual transport rates will be achieved during shorter periods of high wind velocities. Contrastingly our fluvial flow rates are low – and it is quite likely that flood flows would be much greater and may cause different impacts. Given how comparatively low flow rates can readily interrupt high aeolian transport rates it is quite likely that hiatus or ephemeral flows may be important in allowing aeolian forces to impact upon the river system.

6. Conclusions

- This paper presents the first combined sand dune/river model to investigate the geomorphic interactions of fluvial and aeolian processes
- Within the model aeolian and fluvial processes are fully coupled and the different rates of process change are reconciled by using different and adaptable time steps
- For the first time, key interactions between fluvial and aeolian processes were identified, including how rivers can readily prevent the progression of sand dunes (even with small flows), how aeolian sediment transport and dunes can deflect and alter river channel path and how dunes cross river channels

- Over time these interactions lead to channel avulsions, indicating how aeolian sediment transport may be a fundamental process affecting avulsion frequency and therefore alter sedimentology and alluvial architectures.
- Importantly, the model results reveal how important it is to look at the interactions of aeolian and fluvial geomorphic processes from dynamic view instead of static

Acknowledgements

The work presented in this paper is a part of the doctoral research of Baoli Liu who is supported by a joint scholarship provided by the University of Hull and the China Scholarship Council. We wish to thank the three anonymous reviewers for their very useful comments and suggestions. The executable files and source code of the combined dune-fluvial model is freely available under a GNU licence from http://www.coulthard.org.uk and https://sourceforge.net/projects/caesar-lisflood/

References

Baas, A.C.W., 2002. Chaos, fractals and self-organization in coastal geomorphology: Simulating dune landscapes in vegetated environments. Geomorphology 48, 309–328. doi:10.1016/S0169-555X(02)00187-3

Baas, A.C.W., Nield, J.M., 2007. Modelling vegetated dune landscapes. Geophys. Res. Lett. 34. doi:10.1029/2006GL029152

Barchyn, T.E., Hugenholtz, C.H., 2012. A new tool for modeling dune field evolution based on an accessible, GUI version of the Werner dune model. Geomorphology 138, 415–419. doi:10.1016/j.geomorph.2011.09.021

Bates, P.D., Horritt, M.S., Fewtrell, T.J., 2010. A simple inertial formulation of the shallow water equations for efficient two-dimensional flood inundation modelling. J. Hydrol. 387, 33–45. doi:10.1016/j.jhydrol.2010.03.027

Bishop, Momiji, H., Carretero-Gonzalez, R., Warren, a, 2002. Modelling desert dune fields based on discrete dynamics. Discret. Dyn. …. doi:10.1080/10260220290013462

Bourke, M.C., Ewing, R.C., Finnegan, D., McGowan, H.A., 2009. Sand dune movement in the Victoria Valley, Antarctica. Geomorphology 109, 148–160. doi:10.1016/j.geomorph.2009.02.028

Carson, M., Kirkby, M., 1972. Hillslope form and process. New York: Cambridge University Press.

463 Castelltort, S., Van Den Driessche, J., 2003. How plausible are high-frequency sediment supply-driven
464 cycles in the stratigraphic record? Sediment. Geol. 157, 3–13. doi:10.1016/S0037-
465 0738(03)00066-6

466 Coulthard, T.J., 2017. CAESAR-Lisflood 1.9b [Data set]. doi:10.5281/ZENODO.321820

467 Coulthard, T.J., 2001. Landscape evolution models: a software review. Hydrol. Process. 173, 165–
468 173. doi:10.1177/089443930101900313

469 Coulthard, T.J., Hancock, G.R., Lowry, J.B.C., 2012. Modelling soil erosion with a downscaled
470 landscape evolution model. Earth Surf. Process. Landforms 37, 1046–1055.
471 doi:10.1002/esp.3226

472 Coulthard, T.J., Hicks, D.M., Van De Wiel, M.J., 2007. Cellular modelling of river catchments and
473 reaches: Advantages, limitations and prospects. Geomorphology 90, 192–207.
474 doi:10.1016/j.geomorph.2006.10.030

475 Coulthard, T.J., Macklin, M.G., 2003. Modeling long-term contamination in river systems from
476 historical metal mining. Geology 31, 451–454. doi:10.1130/0091-
477 7613(2003)031<0451:MLCIRS>2.0.CO;2

478 Coulthard, T.J., Macklin, M.G., 2001. How sensitive are river systems to climate and land-use
479 changes? A model-based evaluation. J. Quat. Sci. 16, 347–351. doi:10.1002/jqs.604

480 Coulthard, T.J., Neal, J.C., Bates, P.D., Ramirez, J., de Almeida, G. a M., Hancock, G.R., 2013.
481 Integrating the LISFLOOD-FP 2D hydrodynamic model with the CAESAR model: Implications for
482 modelling landscape evolution. Earth Surf. Process. Landforms 38, 1897–1906.
483 doi:10.1002/esp.3478

484 Coulthard, T.J., Van De Wiel, M.J., 2012. Modelling river history and evolution. Philos. Trans. R. Soc.
485 A Math. Phys. Eng. Sci. 370, 2123–2142. doi:10.1098/rsta.2011.0597

486 Coulthard, T.J., Van De Wiel, M.J., 2007. Quantifying fluvial non linearity and finding self organized
487 criticality? Insights from simulations of river basin evolution. Geomorphology 91, 216–235.
488 doi:10.1016/j.geomorph.2007.04.011

489 Coulthard, T.J., Van De Wiel, M.J., 2006. A cellular model of river meandering. Earth Surf. Process.
490 Landforms 31, 123–132. doi:10.1002/esp.1315

491 Davies, N.S., Gibling, M.R., 2010a. Paleozoic vegetation and the Siluro-Devonian rise of fluvial lateral
492 accretion sets. Geology 38, 51–54. doi:10.1130/G30443.1

493 Davies, N.S., Gibling, M.R., 2010b. Cambrian to Devonian evolution of alluvial systems: The
494 sedimentological impact of the earliest land plants. Earth-Science Rev. 98, 171–200.

495 doi:10.1016/j.earscirev.2009.11.002

496 Eastwood, E., Nield, J., Baas, A., Kocurek, G., 2011. Modelling controls on aeolian dune-field pattern
497 evolution. Sedimentology 58, 1391–1406. doi:10.1111/j.1365-3091.2010.01216.x

498 Einstein, H.A., 1950. The bed-load function for sediment transport in open channel flows, in:
499 Technical Bulletin No. 1026, USDA Soil Conservation Service. U.S. Department of Agriculture, p.
500 71.

501 Hancock, G.R., Coulthard, T.J., Martinez, C., Kalma, J.D., 2011. An evaluation of landscape evolution
502 models to simulate decadal and centennial scale soil erosion in grassland catchments. J. Hydrol.
503 398, 171–183. doi:10.1016/j.jhydrol.2010.12.002

504 Hancock, G.R., Lowry, J.B.C., Coulthard, T.J., Evans, K.G., Moliere, D.R., 2010. A catchment scale
505 evaluation of the SIBERIA and CAESAR landscape evolution models. Earth Surf. Process.
506 Landforms 35, 863–875. doi:10.1002/esp.1863

507 Hollands, C.B., Nanson, G.C., Jones, B.G., Bristow, C.S., Price, D.M., Pietsch, T.J., 2006. Aeolian-fluvial
508 interaction: Evidence for Late Quaternary channel change and wind-rift linear dune formation
509 in the northwestern Simpson Desert, Australia. Quat. Sci. Rev. 25, 142–162.
510 doi:10.1016/j.quascirev.2005.02.007

511 Howard, a. D., Morton, J.B., Gad-El-Hak, M., Pierce, D.B., 1978. Sand transport model of barchan
512 dune equilibrium. Sedimentology 25, 307–338. doi:10.1111/j.1365-3091.1978.tb00316.x

513 Hugenholtz, C.H., Levin, N., Barchyn, T.E., Baddock, M.C., 2012. Remote sensing and spatial analysis
514 of aeolian sand dunes: A review and outlook. Earth-Science Rev. 111, 319–334. doi:Doi
515 10.1016/J.Earscirev.2011.11.006

516 Jones, L.S., Blakey, R.C., 1997. Eolian-fluvial interaction in the Page Sandstone (Middle Jurassic) in
517 south-central Utah, USA — a case study of erg-margin processes. Sediment. Geol. 109, 181–
518 198. doi:10.1016/S0037-0738(96)00044-9

519 Kroy, K., Sauermann, G., Herrmann, H.J., 2002. Minimal model for sand dunes. Phys. Rev. Lett. 88,
520 54301. doi:10.1103/PhysRevLett.88.054301

521 Langford, R.P., Chan, M. a., 1989. Fluvial-aeolian interactions: Part II, ancient systems.
522 Sedimentology 36, 1037–1051. doi:10.1111/j.1365-3091.1989.tb01541.x

523 Larsen, L., Thomas, C., Eppinga, M., Coulthard, T., 2014. Exploratory modeling: Extracting causality
524 from complexity. Eos (Washington. DC). 95, 285–286. doi:10.1002/2014EO320001

525 Li, S., Dong, G., Shen, J., Yang, P., Liu, X., Wang, Y., Jin, H., Wang, Q., 1999. Formation mechanism and
526 development pattern of aeolian sand landform in Yarlung Zangbo River valley. Sci. China Ser. D

527 Earth Sci. 42, 272–284. doi:10.1007/BF02878964

528 Liu, B., Coulthard, T.J., 2015. Mapping the interactions between rivers and sand dunes: Implications
529 for fluvial and aeolian geomorphology. Geomorphology 231, 246–257.
530 doi:10.1016/j.geomorph.2014.12.011

531 Livingstone, I., Wiggs, G.F.S., Weaver, C.M., 2007. Geomorphology of desert sand dunes: A review of
532 recent progress. Earth-Science Rev. 80, 239–257. doi:10.1016/j.earscirev.2006.09.004

533 Loope, D.B., Swinehart, J.B., Mason, J.P., 1995. Dune-dammed palaeovalleys of the Nebraska Sand
534 Hills: intrinsic versus climatic controls on the accumulation of lake and marsh sediments. Geol.
535 Soc. Am. Bull. 107, 396–406. doi:10.1130/0016-7606(1995)107<0396:DDPOTN>2.3.CO

536 Maroulis, J.C., Nanson, G.C., Price, D.M., Pietsch, T., 2007. Aeolian-fluvial interaction and climate
537 change: source-bordering dune development over the past ???100 ka on Cooper Creek, central
538 Australia. Quat. Sci. Rev. 26, 386–404. doi:10.1016/j.quascirev.2006.08.010

539 Mazzullo, J.M., Ehrlich, R., 1983. Grain-shape variation in the St. Peter Sandstone; a record of eolian
540 and fluvial sedimentation of an early Paleozoic cratonic sheet sand. J. Sediment. Res. 53, 105–
541 119. doi:10.1306/212F8161-2B24-11D7-8648000102C1865D

542 Momiji, H., Warren, A., 2000. Relations of sand trapping efficiency and migration speed of transverse
543 dunes to wind velocity. Earth Surf. Process. Landforms 25, 1069–1084. doi:10.1002/1096-
544 9837(200009)25:10<1069::AID-ESP117>3.0.CO;2-D

545 Muhs, D.R., Reynolds, R.L., Been, J., Skipp, G., 2003. Eolian sand transport pathways in the
546 southwestern United States : importance of the Colorado River and local sources importance of
547 the Colorado River and local sources. Quat. Int.

548 Murray, a. B., Paola, C., 1997. Properties of a cellular braided-stream model. Earth Surf. Process.
549 Landforms 22, 1001–1025. doi:10.1002/(SICI)1096-9837(199711)22:11<1001::AID-
550 ESP798>3.3.CO;2-F

551 Murray, a. B., Paola, C., 1994. A cellular model of braided rivers. Nature 371, 54–57.
552 doi:10.1038/371054a0

553 Narteau, C., Zhang, D., Rozier, O., Claudin, P., 2009. Setting the length and time scales of a cellular
554 automaton dune model from the analysis of superimposed bed forms. J. Geophys. Res. Solid
555 Earth 114. doi:10.1029/2008JF001127

556 Nicholas, A.P., 2005. Cellular modelling in fluvial geomorphology. Earth Surf. Process. Landforms 30,
557 645–649. doi:10.1002/esp.1231

558 Nield, J.M., Baas, a. C.W., 2008. Investigating parabolic and nebkha dune formation using a cellular

559 automaton modelling approach. Earth Surf. Process. Landforms 33, 724–740.
560 doi:10.1002/esp.1571

561 Nishimori, H., Yamasaki, M., Andersen, K.H., 1998. A Simple Model for the Various Pattern Dynamics
562 of Dunes. Int. J. Mod. Phys. B 12, 257–272. doi:10.1142/S021797929800020X

563 Ouichi, N.B., Nishimori, H., 1995. Modelling of wind-blown sand using cellular automata. Phys. Rev. E
564 52, 5877–5880.

565 Parteli, E.J.R., Herrmann, H.J., 2003. A simple model for a transverse dune field. Phys. A Stat. Mech.
566 its Appl. 327, 554–562. doi:10.1016/S0378-4371(03)00512-0

567 Parteli, E.J.R., Kroy, K., Tsoar, H., Andrade, J.S., Pöschel, T., 2014. Morphodynamic modeling of
568 aeolian dunes: Review and future plans. Eur. Phys. J. Spec. Top. 223, 2269–2283.
569 doi:10.1140/epjst/e2014-02263-2

570 Pelletier, J.D., 2009. Controls on the height and spacing of eolian ripples and transverse dunes: A
571 numerical modeling investigation. Geomorphology 105, 322–333.
572 doi:10.1016/j.geomorph.2008.10.010

573 Roskin, J., Tsoar, H., Porat, N., Blumberg, D.G., 2011. Palaeoclimate interpretations of Late
574 Pleistocene vegetated linear dune mobilization episodes: Evidence from the northwestern
575 Negev dunefield, Israel. Quat. Sci. Rev. 30, 3364–3380. doi:10.1016/j.quascirev.2011.08.014

576 Smith, N.D., Smith, D.G., 1984. William River: an outstanding example of channel widening and
577 braiding caused by bed-load addition (Saskatchewan, Canada). Geology 12, 78–82.
578 doi:10.1130/0091-7613(1984)12<78:WRAOEO>2.0.CO;2

579 Song, Y., Yan, P., Liu, L., 2006. A review of the research on complex erosion by wind and water. J.
580 Geogr. Sci. 16, 231–241. doi:10.1007/s11442-006-0212-1

581 Sweet, M.L., Nielson, J., Havholm, K., Farrelly, J., 1988. Algodones dune field of southeastern
582 California: case history of a migrating modern dune field. Sedimentology 35, 939–952.
583 doi:10.1111/j.1365-3091.1988.tb01739.x

584 Tastet, J.P., Pontee, N.I., 1998. Morpho=chronology of coastal dunes in Medoc. A new interpretation
585 of Holocene dunes in southwestern France. Geomorphology 25, 93–109. doi:10.1016/S0169-
586 555X(98)00035-X

587 Thomas, R., Nicholas, a. P., 2002. Simulation of braided river flow using a new cellular routing
588 scheme. Geomorphology 43, 179–195. doi:10.1016/S0169-555X(01)00128-3

589 Thomas, R., Nicholas, a. P., Quine, T. a., 2007. Cellular modelling as a tool for interpreting historic
590 braided river evolution. Geomorphology 90, 302–317. doi:10.1016/j.geomorph.2006.10.025

591 Tucker, G.E., Hancock, G.R., 2010. Modelling landscape evolution. Earth Surf. Process. Landforms 35,
592 28–50. doi:10.1002/esp.1952

593 Van De Wiel, M.J., Coulthard, T.J., Macklin, M.G., Lewin, J., 2007. Embedding reach-scale fluvial
594 dynamics within the CAESAR cellular automaton landscape evolution model. Geomorphology
595 90, 283–301. doi:10.1016/j.geomorph.2006.10.024

596 Veiga, G.D., Spalletti, L.A., Flint, S., 2002. Aeolian/fluvial interactions and high-resolution sequence
597 stratigraphy of a non-marine lowstand wedge: the Avile Member of the Agrio Formation
598 (Lower Cretaceous), central Neuquen Basin, Argentina. Sedimentology 49, 1001–1019.
599 doi:10.1046/j.1365-3091.2002.00487.x

600 Vermeesch, P., Drake, N., 2008. Remotely sensed dune celerity and sand flux measurements of the
601 world's fastest barchans (Bod??l??, Chad). Geophys. Res. Lett. 35, L24404.
602 doi:10.1029/2008GL035921

603 Welsh, K.E., Dearing, J. a., Chiverrell, R.C., Coulthard, T.J., 2009. Testing a cellular modelling approach
604 to simulating late-Holocene sediment and water transfer from catchment to lake in the French
605 Alps since 1826. The Holocene 19, 785–798. doi:10.1177/0959683609105303

606 Werner, B.T., 1995. Eolian dunes: computer simulations and attractor interpretations. Geology 23,
607 1107–1110. doi:10.1130/0091-7613(1995)023<1107:edcsaa>2.3.co;2

608 Wilcock, P.R.P., Crowe, J.J.C., 2003. Surface-based transport model for mixed-size sediment. J.
609 Hydraul. Eng. 129, 120–128. doi:10.1061/(ASCE)0733-9429(2003)129:2(120)

610 Willgoose, G., 2005. Mathematical Modeling of Whole Landscape Evolution. Annu. Rev. Earth Planet.
611 Sci. 33, 443–459. doi:10.1146/annurev.earth.33.092203.122610

612 Wippermann, F.K., Gross, G., 1986. The wind-induced shaping and migration of an isolated dune: A
613 numerical experiment. Boundary-Layer Meteorol. 36, 319–334. doi:10.1007/BF00118335

614 Zhang, D., Narteau, C., Rozier, O., Courrech du Pont, S., 2012. Morphology and dynamics of star
615 dunes from numerical modelling. Nat. Geosci. doi:10.1038/ngeo1503

616